Journal of Sustainable Metallurgy (2023) 9:52–65
https://doi.org/10.1007/s40831-023-00647-8

SHORT COMMUNICATION

Investigation of the Contents of the Stack Emissions of Iron Ore Sinter Plants With and Without Bag Filter

Veera Brahmacharyulu Angalakuditi[1] · Karthik Bappakan[1] · Sudhakar Karre[1] · Krishna Rao Muppuri[1] · Lokendra Raj Singh[1]

Received: 8 October 2022 / Accepted: 2 January 2023 / Published online: 20 January 2023
© The Minerals, Metals & Materials Society 2023

Abstract

This investigation aims to identify the reasons for the plumes' visibility, compare the stacks with other sinter plant stacks worldwide, and suggest countermeasures to completely stop the visibility of emissions. The appearance of the sinter plant stack emission changes with time and the background color of the sky due to the scattering effect of the sunlight and incidence angle. The flue gas samples were collected at the outlet of the emission control equipment and observed under optical and scanning electron microscopes. The characterization was performed with the help of an electron dispersive spectroscope and mapping technique. The contents of the stack of a sinter plant without a bag filter had much higher levels of PM_{10}, $SO_{2,}$ and NO_x. The emissions from all the sinter plants were invariably found to have particulates of SO_2 and NO_x of size less than 2.5 microns. It is suggested to opt for state-of-the-art fabric filter technology to eliminate $PM_{2.5}$ emissions also.

The contributing editor for this article was Il Sohn.

✉ Veera Brahmacharyulu Angalakuditi
angalakuditi.brahmacharyulu@jsw.in;
avb.acharyulu@gmail.com

1 JSW Steel Ltd, Vijayanagar Works, Ballari, Karnataka 583275, India

Graphical Abstract

Keywords Particulates · Plume visibility · Sunlight scattering · MEROS · HTBF · Bag filter

Introduction

The stack emissions of the iron ore sinter plant contain flue gas with CO, CO_2, H_2O vapors; fine particles of iron ore, sinter components; and particulates of SO_x, NO_x, KCl, and PCDD/Fs. The appearance of the stack emissions varies with the plume contract, its contents, and the meteorological conditions, especially sunlight intensity, scattering, time, the relative humidity in the atmosphere, and the background color of the sky [1]. In other words, it is the overall experience of the observer depending upon his position against the sun, apart from the contents of the flue gas. The plume visibility of the sinter plants with varying sky colors and different times is depicted in Figs. 1, 2, and 3.

The research conducted at ArcelorMittal CST, Brazil, and the Federal University of Espirito Santo between 1998 and 2006 revealed that higher NO_x emissions above 400 mg/Nm^3 increased the plume visibility [2]. The sinter plume visibility was investigated at Nippon Steel Nagoya works in 2006 [3] and Tata Steel, Port Talbot in 2011 [4]. Kasama et al. [3] attributed the visibility largely to the dust concentration. It was indicated that the condensed mist of SO_3 and HCl could appear as white smoke. The recent research in China using a pot sinter arrangement indicated that there is a distinct similarity between $PM_{2.5}$ and SO_x emissions [5]. According to the fundamental principles of light scattering and visibility of gases and particulates, the primary particles of SO_2 ad NO do not bear any effect on the visibility. They are converted to SO_4 aerosols and NO_2 gas which absorb

Fig. 1 Plume visibility with varying background color **a** slightly reddish and whitish appearance in the afternoon blue background, **b** reddish and white plume in the morning blue background, **c** white plume in the night sky, **d** downwash of white plume in the night sky, **e** mixture of a reddish and white plume in the night sky (Color figure online)

the light. NO_2 is further converted to HNO_3, which does not absorb or scatter light. Further, ammonium nitrate scatters the light. The scattering of the light from the particles suspended in the air is a function of the wavelength, their refractive index, and polarization [1] known as the Rayleigh effect. The intensity of the reflected light is inversely proportional to the fourth power of the wavelength. The blue light is more strongly visible than the red light. For particles of larger size (non-molecular/aerosols), Mie scattering principles are applicable. Greater the size of the particle, the more its radiation in the forward direction than in the reverse direction. Tyndall effect refers to the scattering by colloidal of 0.04 to 0.9-micron size, and the changing appearance (color) from different angles or locations of the observer. According to this effect, the smoke appearing blue from one angle may appear red from a different angle from a distance. Hence the blue-red ratio and color contrast parameter are included in the plume visibility models [6]. The wavelength of infrared light is in the range of 0.7 to 1 micron, visible light 0.03 to 0.7 microns, and ultraviolet light 0.01 to 0.4 microns. The changing appearance of the scattered light through the particulates of size equal to one-fourth of the wavelength applies to all of the above radiations. Particulates larger than the above size may reflect the light normally. In our experience, the yellowish appearance intensifies when the volatile matter in the solid fuel increases.

The emissions from the stacks of sinter plants have reddish dust; yellowish and white fumes/particulates. Our sinter plants have one ESP to filter the process gas and one ESP for de-dusting each. The filtered gas joins a common stack (excepting one sinter plant, without a bag filter). A sinter plant has maximized emission reduction of sintering (MEROS) and

Fig. 2 Stack emissions **a** afternoon hours, reddish and yellowish appearance, **b** reddish, whitish appearance, morning hours, **c** yellowish appearance evening hours, observer facing the sun, **d** reddish appearance, morning hours (Color figure online)

Fig. 3 Stack emissions **a, b** reddish and whitish appearance, afternoon hours, **c** reddish appearance, evening hours, as seen from the east side, **d** whitish appearance in a cloudy weather (Color figure online)

waste gas recycling (WGR) and another one high-temperature bag filter (HTBF). The contents of the stack emissions are a combination of process fumes and de-dusting dust. The reddish appearance is due to the dust particles containing micro fines of iron ore that either leak through the sinter bed or are captured by the de-dusting system. An efficient ESP should be able to filter these particles (100 to 150-micron size). The volatile matter (VM) in the solid fuel renders yellowish fumes containing volatile organic compounds (VOCs), poly chlorinated biphenyls (PCBs), and polycyclic aromatic hydrocarbons

Table 1 Various emission reduction schemes installed worldwide

Country	Company	Scheme/countermeasure
Japan	JFE, Chiba No. 4	Lime, gypsum injection for De-SO*x*, De-NO*x*, and Dioxins
	JFE, Keihin No. 1	Ammonia absorption
	JFE, Kurashiki	Magnesium hydroxide injection
	JFE, Fukuyama	Additional High-performance ESPs, Activated carbon, De-SO*x*, De-NO*x*
	Kobe Steel, Kakogawa	High-performance ESPs, De-SO*x*, and De-NO*x* facilities
	Nippon Steel, Tobata, Oita	Waste gas recirculation system, Bag Filter, DE-SO*x*, De-NO*x*
South Korea	POSCO, Pohang and Gwangyang	Anthracite, selective ctalytic reduction (SCR), ESP dust recycling, Bag Filter
Netherlands	Tata Steel, Ijmuiden	Lignite, Lime, Urea injection, and De-SO*x*
UK	Tata Steel, Port Talbot	Advanced ESP, Urea & Lignite injection, De-SO*x*
Austria	Voestalpine Stahl, Linz	MEROS + EPOSint-selective waste gas recycling
Luxembourg	ArcelorMittal, Belval	–
Spain	ArcelorMittal, Gijón	Electro-filter, sleeve bag filter
	AreclorMittal, Astrurias	New Bag Filter
France	AreclorMittal, Mediterrannee	New Bag Filter
Germany	Thyssenkrupp Stahl, Duisburg	De-SO*x*, De-NO*x*, World's largest (32 m) fabric filter
	Eisenhuttenstahl	Chlorine control, Lignite Injection
Belgium	ArcelorMittal, Gent	EOS, Hybrid Electro-filter
Bosnia & Herzegovina	ArcelorMittal, Zenica	Hybrid Filter of FLSmidth
Ukraine	ArcelorMittal, Kryvyi Rih	Reconstruction of ESPs (new)
Kazakhstan	ArcelorMittal Temirtau	Reconstruction of ESPs (new)
Brazil	ArcelorMittal, CSN	MEROS
	ArcelorMittal, Tubarão	Preventive Maintenance (SISMAN, SISPAD)
	CSP	ESP revamp
	Usiminas	ESP revamp
Australia	Bluescope, Kembla	Activated carbon tower

(PAHs). The higher the VM, the greater the yellowish appearance of the fume. Chlorine in the raw materials generates KCl and polychlorinated di-benzo dioxins/furans (PCDD/Fs). Interested readers may refer to our earlier research [7]. CO_2 emissions appear blue [8]. Sulfur and nitrogen in the raw materials (especially solid fuel) result in SO_x and NO_x emissions. These particulates appear white. The literature indicates the photo-oxidation of SO_2 with OH radicals to form SO_3, as the main reason for the whitish plume visibility [9, 10].

The literature that appeared during 1972–1978 indicates that the bag filters were successfully operated in Indiana and Fontana with strict control of the oil content in the mill scale. The oil in the mill scale generates hydrocarbons and increases the chances of a fire in the dust hoppers [11]. The emissions from the stacks of the sinter plants the world over have visible white/blue smoke and sometimes yellowish/reddish particles; the intensity is varying, though. A wide variety of particulate emission control systems are installed worldwide including expensive selective catalytic reactors (SCR). Waste Gas Recycling (WGR), activated carbon/lignite towers, maximized emission reduction of sintering (MEROS), and emission optimized sintering (EOS) are some of the popular advanced technologies. From the literature and the developments elsewhere in the world, it is understood that the world's largest hybrid fabric filter developed in collaboration between ThyssenKrupp and FLSmidth is very effective, as installed in the sinter plant of ThyssenKrupp, Duisburg [12]. It was installed along with a 100-m tall stack. It is suggested to install it, as a long-term solution.

The various schemes for addressing the visible stack emissions worldwide are provided in Table 1. The hybrid fabric filter installed in ThyssenKrupp is claimed to be effective for all varieties of emissions. Oxy-fuel burners have low NO_x emissions and are being considered to address the NO_x emissions from the ignition furnace.

Investigation Methodology

The samples of the flue gas were collected after the MEROS, the HTBF, and the ESPs separately. The manual isokinetic stack monitoring equipment (Ecotech Stack Sampler ESS100 model and its kit) was used for this purpose, whose image is provided in Fig. 4a. This apparatus cannot determine SO_3 content separately.

The deposits in the thimbles (as shown in Fig. 4b), after the sample collection is over, are observed under the

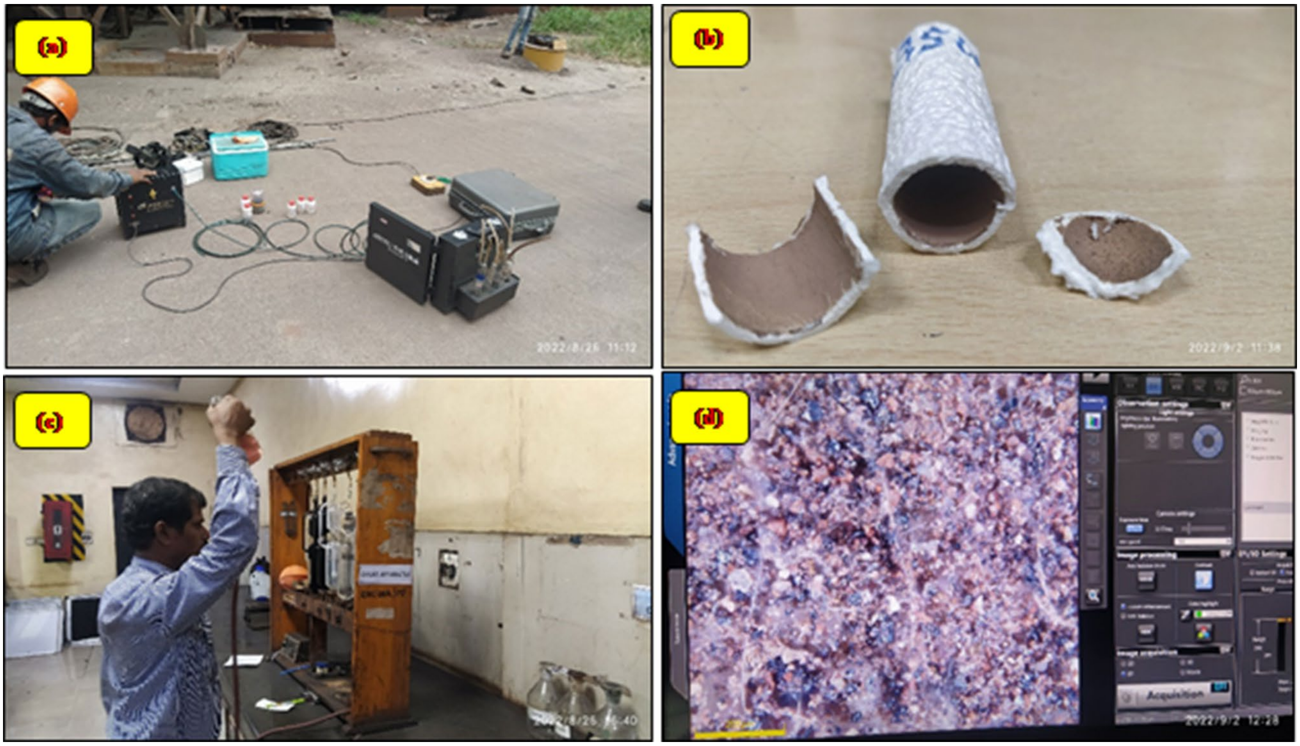

Fig. 4 **a** Stack sampler kit, **b** the deposit of particulates in a thimble, **c** Orsat apparatus, **d** optical micrograph

Table 2 SO_2, NO_x, and PM_{10} in the stacks of sinter plants

S.No	Sample identity	Date	Time	SO_2 (mg/Nm^3)	NO_x (mg/Nm^3)	PM (mg/Nm^3)
1	MEROS outlet sample-1	26.08.2022	12:45 PM–01:45 PM	23.0	28.4	65.0
2	MEROS outlet sample-2	26.08.2022	11:40 AM–12:40 PM	19.8	26.8	48.0
3	HTBF outlet sample-1	26.08.2022	02:30 PM–04:30 PM	32.6	39.6	3.0
4	HTBF outlet sample-2	26.08.2022	04:30 PM–05:30 PM	43.7	47.5	5.0
5	ESP-1 outlet sample-1	27.08.2022	02:10 PM–03:40 PM	10.1	36.2	42.0
6	ESP-1 outlet sample-2	27.08.2022	11:20 AM–12:50 PM	7.80	28.6	46.0
7	ESP-2 outlet sample-1	27.08.2022	11:25 AM–12:55 PM	55.5	82.1	371.0
8	ESP-2 outlet sample-2	27.08.2022	02:20 PM–03:40 PM	42.0	71.3	78.0
9	HTBF outlet sample-3	02.09.2022	03:50 PM–05:50 PM	218.3	445.7	29.0
10	ESP-1 outlet sample-3	03.09.2022	11:24 PM–12:54 PM	132.9	181.9	39.0
11	ESP-2 outlet sample-3	03.09.2022	11:22 AM–12:52 PM	250.2	474.5	57.0
12	MEROS outlet sample-3	03.09.2022	02:55 PM–03:55 PM	228.9	405.8	57.0

Table 3 Analysis of the flue gas as quantified with the help of the Orsat apparatus

S.no.	Sample identity	Date	Time	CO_2%	CO%	O_2%	H_2%
1	MEROS outlet sample-1	26.08.2022	12:45 PM–01:45 PM	1.60	0.20	19.40	1.40

Olympus optical microscope and EDAX scanning electron microscope. The flue gas analysis was obtained with the help of the Orsat apparatus located in the QMC laboratory (Fig. 4c). The bladder used for monitoring the fuel gases was used to collect the flue gas sample. The vacuum pump of a 50 L per minute capacity of the stack sampler was used for this purpose. The salient elements of the kit are given below.

1. Thimble (PM_{10} by weight loss method)

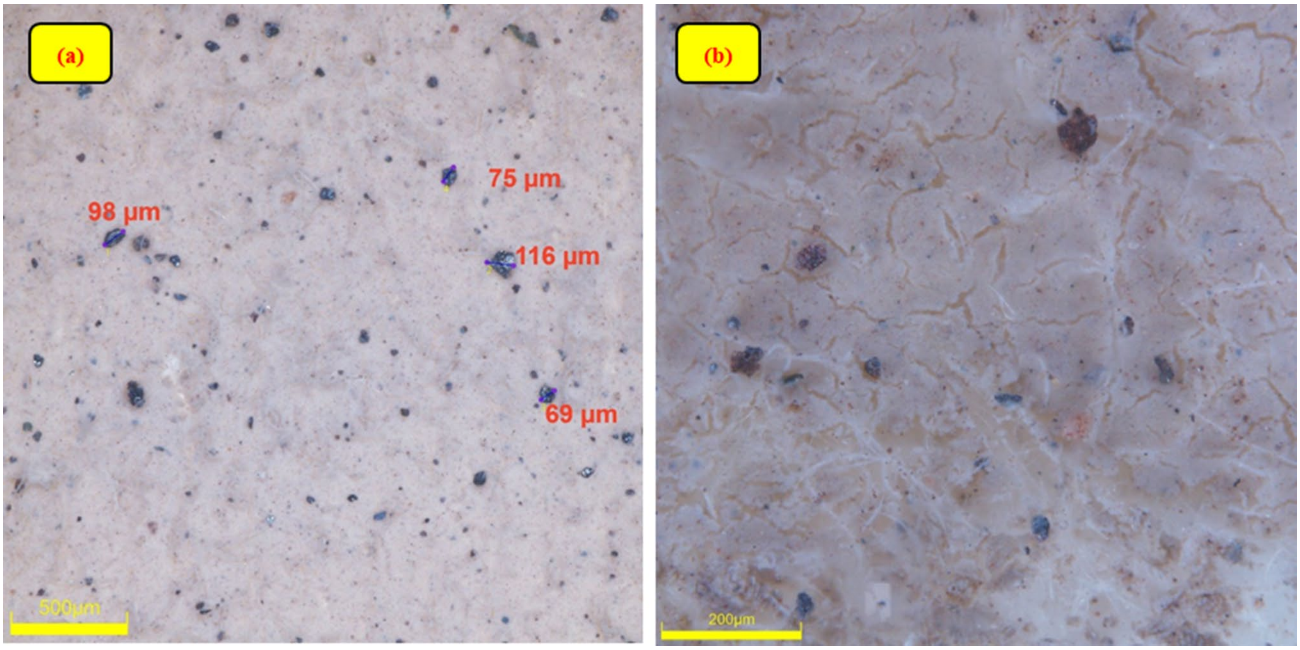

Fig. 5 MEROS outlet thimble deposit **a** at ×100 magnification, **b** at ×300 magnification

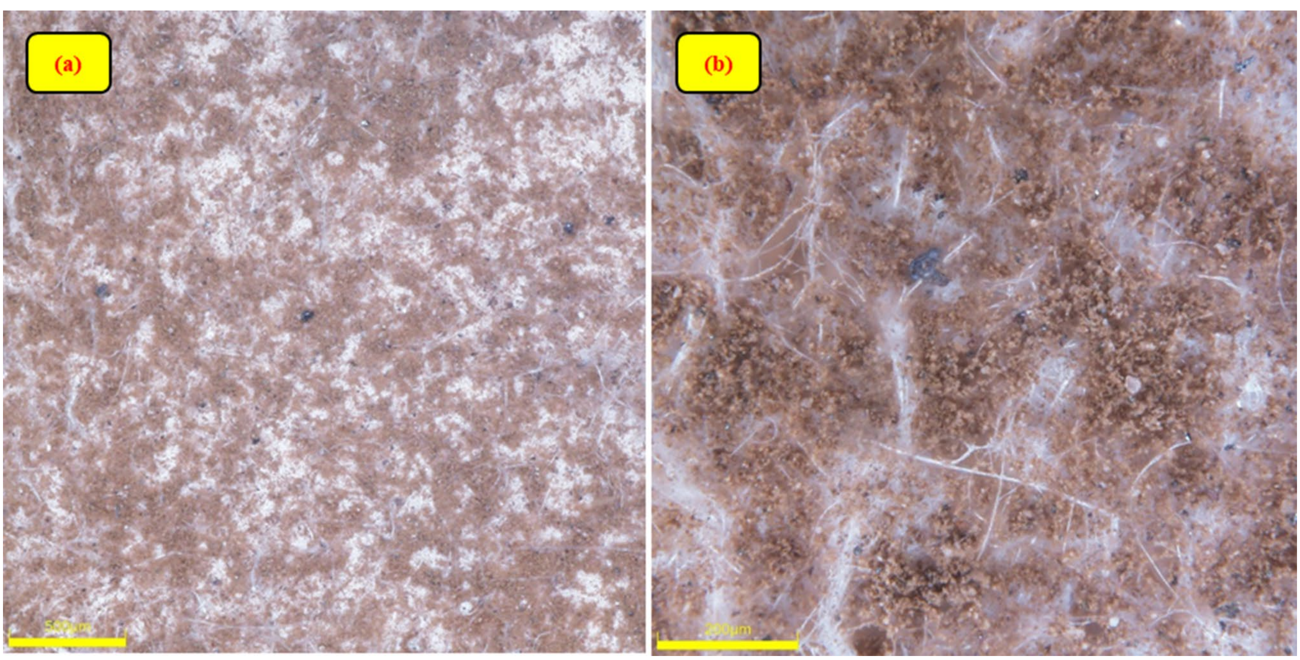

Fig. 6 HTBF outlet thimble deposit **a** at ×100 magnification, **b** at ×300 magnification

2. Three impingers to capture SO_2, NO_x, and H_2O with the help of reagents
    a. Isopropanol alcohol (reagent for NO_x)
    b. Hydrogen peroxide (oxidizer, reagent to absorb SO_2)
    c. Silica gel to absorb H_2O
3. Vacuum pump

Results and Discussion

The results of the stack monitoring, optical microscopy, scanning electron microscopy and electron dispersive spectroscopy mapping are provided in this section.

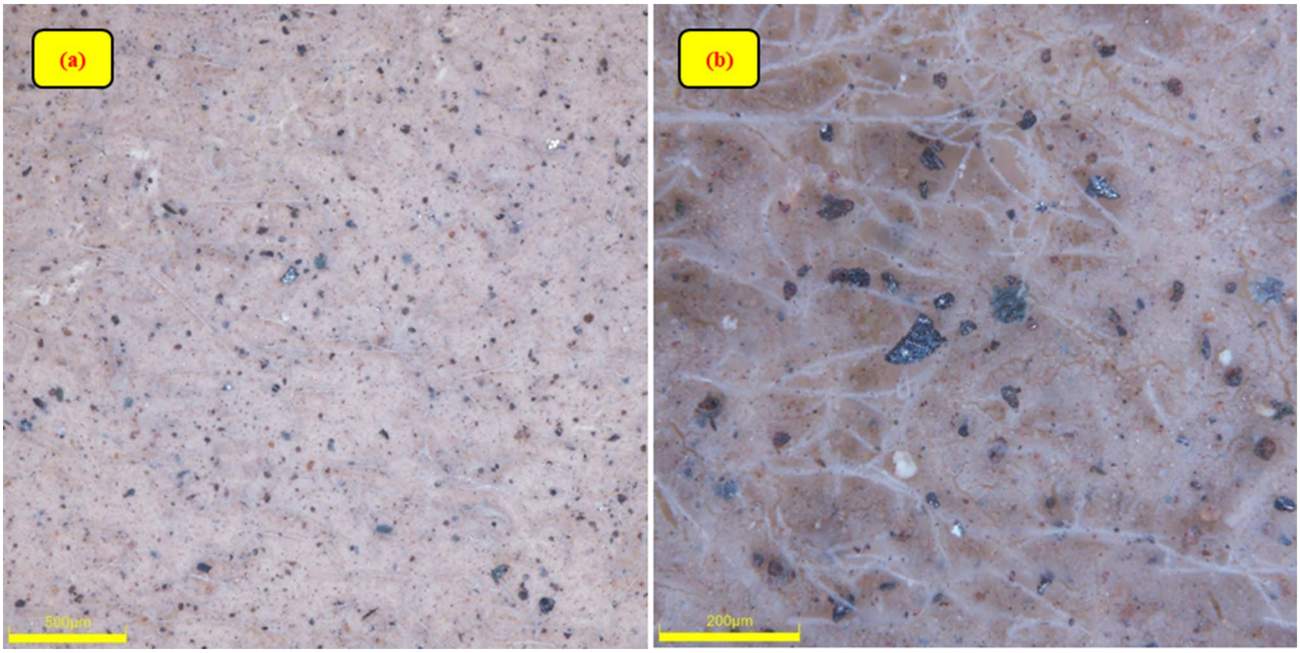

Fig. 7 ESP-1 outlet thimble deposit **a** at ×100 magnification, **b** at ×300 magnification

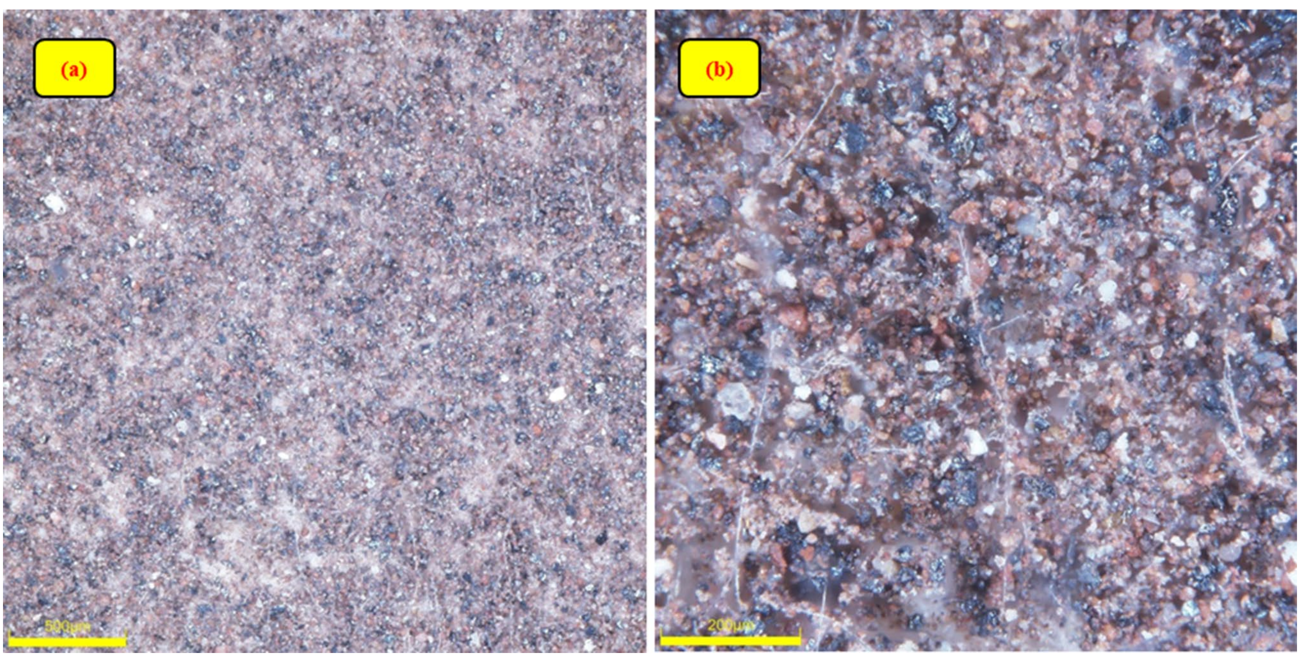

Fig. 8 ESP-2 outlet thimble deposit **a** at ×100 magnification, **b** at ×300 magnification

Stack Monitoring

The results of the monitoring exercise are provided in Table 2. The analysis of the flue gas is given in Table 3.

Optical Microscopy

The appearance of the entrapped particles in the thimbles is shown in Figs. 5, 6, 7, and 8. The size of the particles varied from 60 to 120 microns. In the case of higher emissions, the background appeared brownish. The fibers of the thimble are appearing as white streaks in the micrographs. The chemical

Table 4 Summary elemental analyses (at%) of the EDS spots in the MEROS, HTBF, and ESP thimbles

Element	N K	O K	NaK	AlK	SiK	S K	ClK	K K	CaK	FeK
MEROS_1	9.54	40.13	6.19	1.62	4.33	2.88	17.88	16.16	1.27	–
MEROS_2	8.17	36.86	5.24	1.66	3.53	3.53	20.79	18.76	1.45	–
MEROS_3	13.67	74.43	1.44	3.08	2.76	0.42	0.78	0.65	2.77	–
MEROS_4	12.35	70.40	0.67	0.27	2.06	1.52	1.15	1.28	10.29	–
MEROS_5	13.74	73.34	1.33	2.44	1.84	1.11	2.61	2.53	1.06	–
HTBF_1	8.41	50.85	0.84	2.52	6.62	0.97	1.90	1.77	15.32	10.81
HTBF_2	7.95	41.42	0.37	1.60	0.78	0.10	1.51	1.71	0.84	43.72
HTBF_3	4.91	34.68	2.69	1.50	8.96	2.96	19.78	20.45	4.07	–
HTBF_4	5.39	30.66	5.42	1.74	12.33	3.20	18.68	18.22	4.36	–
HTBF_5	5.81	34.77	5.82	1.59	11.30	2.93	17.00	16.66	4.12	–
ESP_1	8.71	38.96	4.25	2.15	3.79	2.47	14.1	14.16	5.50	5.91
ESP_2	9.36	51.01	1.53	7.95	9.84	1.65	6.14	5.06	3.14	4.33
ESP_3	3.05	27.32	3.88	1.65	8.20	2.78	17.29	16.33	8.38	11.11
ESP_4	2.13	29.19	3.69	4.42	7.41	3.14	11.62	10.64	8.42	19.34
ESP_5	6.62	39.57	3.89	1.86	6.51	1.87	10.71	9.92	7.49	11.57
ESP_6	13.19	58.03	1.11	9.51	9.62	0.46	2.74	3.05	0.90	1.39
ESP_7	12.13	62.13	0.91	10.75	9.41	0.34	1.12	1.06	0.75	1.41
ESP_8	7.27	39.05	4.30	2.73	6.43	2.04	12.25	11.49	6.57	7.87
ESP_9	3.66	36.30	3.92	1.57	9.47	2.26	10.07	7.19	20.34	5.21
ESP_10	10.09	41.24	4.37	1.62	3.89	2.73	13.17	12.57	5.71	4.61
ESP_11	12.54	54.22	1.65	1.30	1.56	0.68	2.29	1.95	2.01	21.8

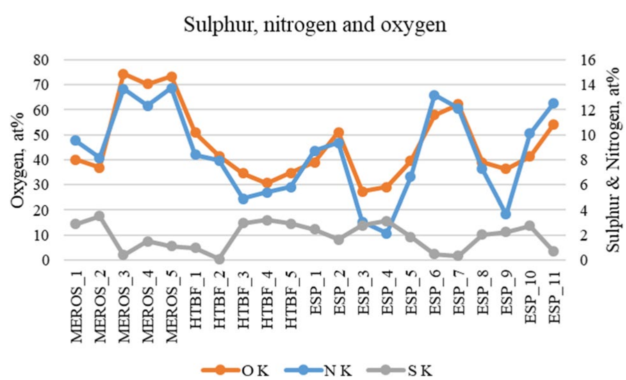

Fig. 9 Proportional variation of oxygen with nitrogen and sulphur, indicating that the particulates have NO_x

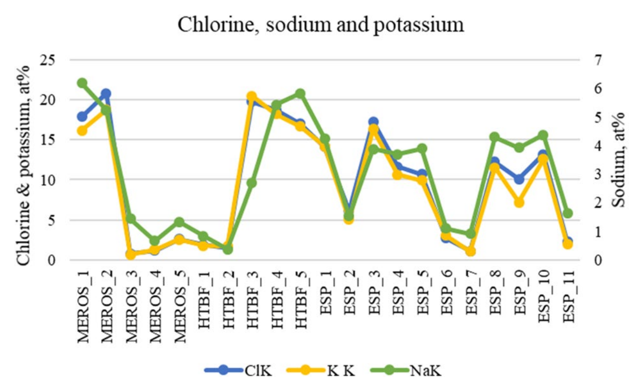

Fig. 10 Proportional variation of chlorine with sodium and potassium, indicating the presence of KCl and NaCl

composition of the particles was investigated with the help of a scanning electron microscope, as discussed in the next section.

Scanning Electron Microscopy

The scanning electron microscopy and the electron dispersive spectroscopy mapping of the deposits in the thimbles were conducted with the help of EDAX. The excitation voltage was set at 10 kV and the mode of detecting the elements was set "automatic". The summary of the spot analyses is given in Table 4. It is observed that the data without a bag filter are different from that with bag filter.

The variation of sulfur and nitrogen are plotted with oxygen to understand the presence of SO_2 and NO_x which is shown in Fig. 9. As nitrogen is in phase with oxygen, it can be understood that NO_x is present. Sulfur is out of phase, rather is forming a mirror image with oxygen. Similarly, chlorine content is plotted against sodium and potassium in Fig. 10. It is evident that all are in phase and therefore can be comprehended that NaCl and KCl are present.

To see if PCDD/Fs are present, chlorine is plotted against oxygen, as shown in Fig. 11. It is out of phase and forming a mirror image. The major elements that constitute the slag phase in the sinter are plotted against oxygen

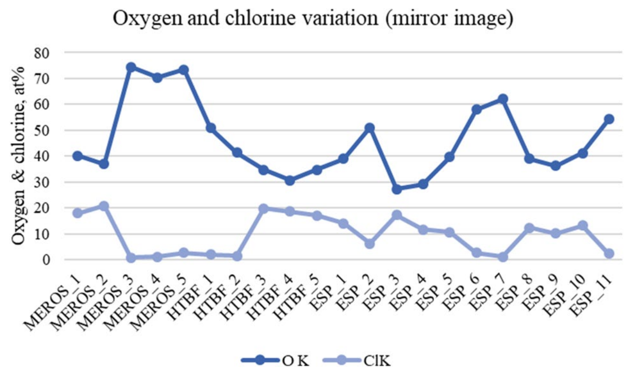

Fig. 11 Variation of oxygen and chlorine (mirror image), indicating that PCDD/Fs may not be present

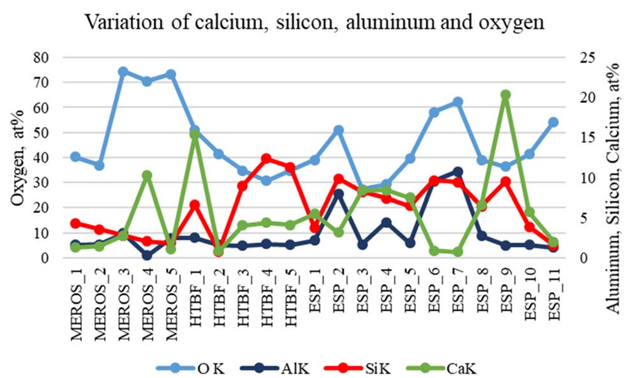

Fig. 12 Variation of oxygen plotted with aluminum, silicon, and calcium; indicating that oxygen is in sync with aluminum; calcium is a mirror image with oxygen, indicating the absence of free CaO

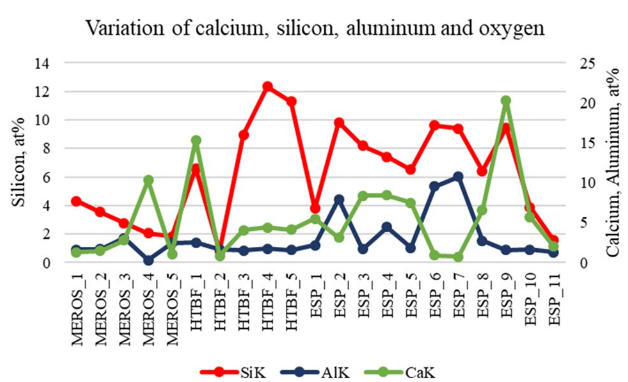

Fig. 13 Variation of aluminum and calcium against silicon; indicating the presence of sinter phase (SFCA) components

and are presented in Figs. 12 and 13. It is noticed that aluminum is in sync with oxygen; silicon and calcium are not. It can be stated that CaO is not present in free form, rather calcium is combined with silicon and aluminum;

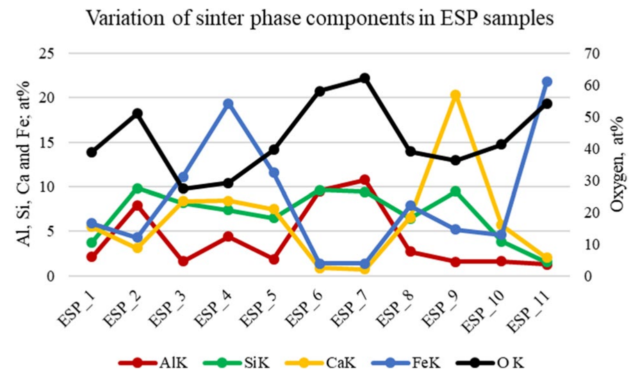

Fig. 14 Variation of sinter components without bag filter (Al and O are directly proportional; Ca and Si are inversely proportional marginally)

indicating the presence of silico ferrites of calcium and aluminum (SFCA) components.

The data without the bag filter have been plotted to see the stoichiometric balance of SFCA components, as shown in Figs. 14 and 15. Ideally, in the slag phase, Fe should diminish as Ca, Si, and Al components increase. A similar trend is noticed in the plot.

The results of the mapping of the MEROS, HTBF, and ESP thimbles are provided in Figs. 16, 17, 18, Tables 5, 6, and 7.

By comparing the elemental analyses of the mapping, it is evident that in the cases of HTBF and ESP, chlorine, potassium, and sulfur are higher. In the case of MEROS, silicon and sodium are higher. Oxygen and calcium are present in all the cases, indicating the traces of lime (the binder) and the calcite component in the sinter. Chlorine is associated with potassium largely, to some extent sodium; but not with oxygen. This confirms the presence of KCl and NaCl, and absence of PCDD/Fs.

Due to the Covid-19 pandemic, the annual maintenance of the pollution control equipment could not be carried out and their effectiveness deteriorated across all the sinter plants. In a sinter plant with MEROS and WGR systems, the filter bags are due to change. Hence, the results of the stack monitoring indicated higher emissions than pre-pandemic times. The unhealthy electrostatic fields in its ESP have resulted in the carry-over of excessive dust load to the bag filter. In the other sinter plant with a new HTBF, the emissions were minimum. The unhealthy electrostatic fields in the ESP may affect the life cycle of the HTBF and MEROS. In a sinter plant without a bag filter, the stack emissions were much higher.

Conclusions

The following conclusions are drawn from the investigation:

1. The differing perception of an observer standing at different locations with respect to the sun, about the color

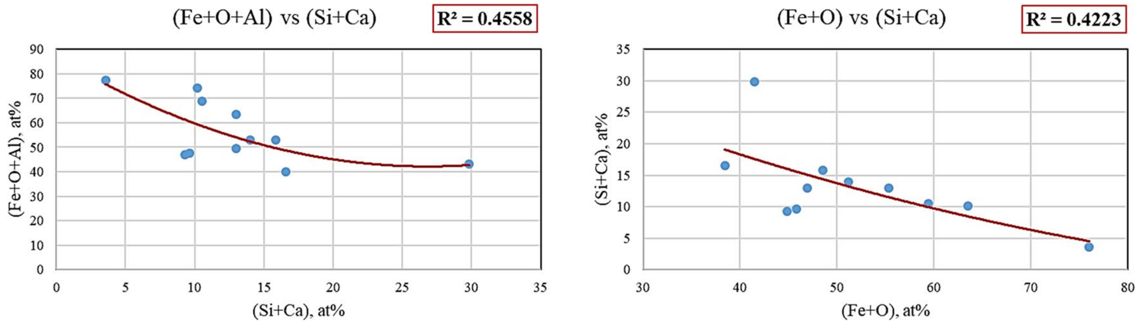

Fig. 15 Scatter plot of (Fe + O + Al) with (Si + Ca) and (Fe + O) with (Si + Ca) in ESP samples

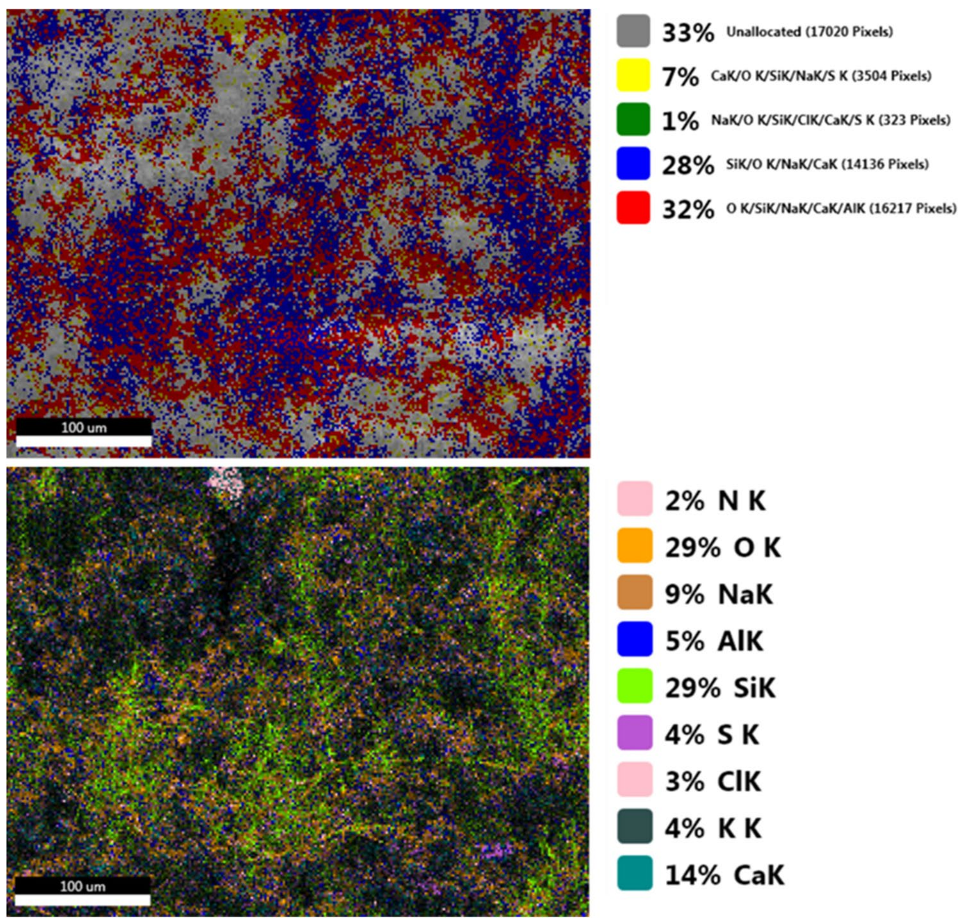

Fig. 16 Mapping of the MEROS thimble

of the sinter plant stack emissions, is explainable with the help of the principles of light scattering.

2. The particles up to 120-micron size are escaping into the atmosphere (up to 300 mg/Nm^3), where only ESP is installed. The content of SO_2 and NO_x is in the tune of 250 and 450 mg/Nm^3, respectively.

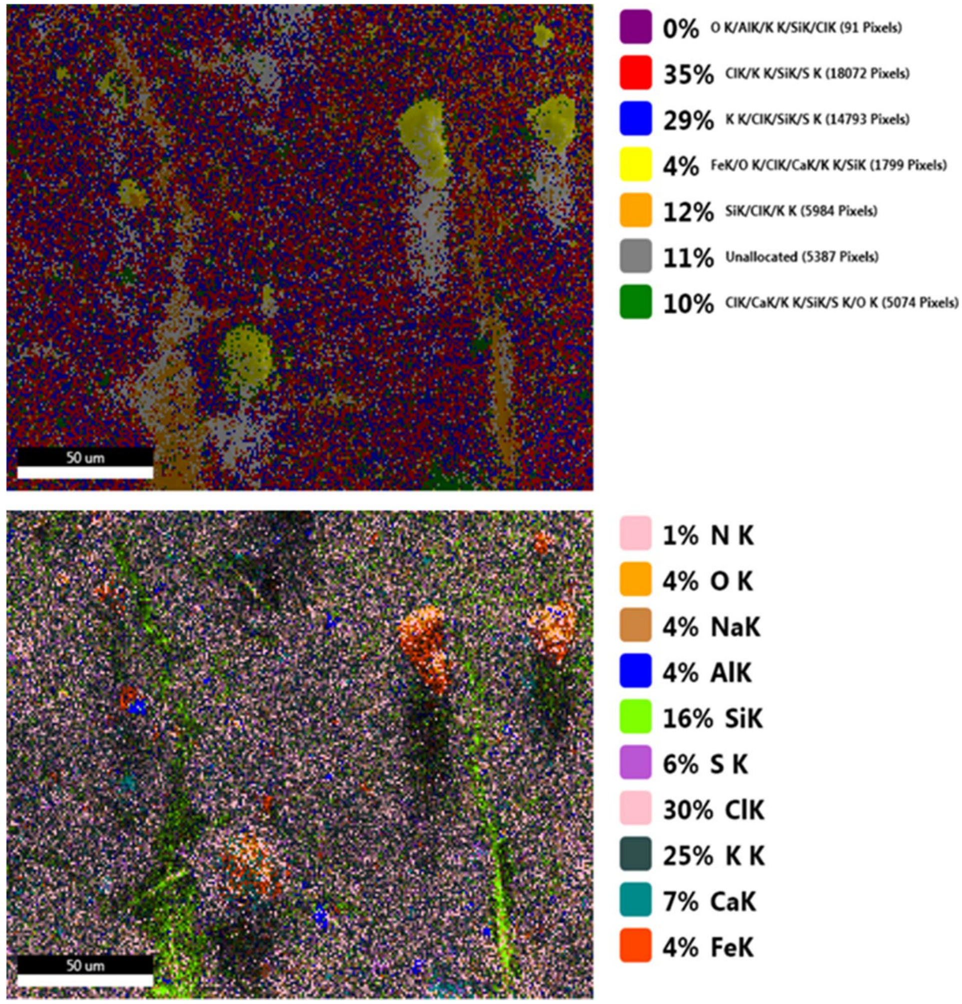

Fig. 17 Mapping of the HTBF thimble

3. The particles of 10-micron size are escaping into the atmosphere through HTBF (20 mg/Nm^3) and MEROS (60 mg/Nm^3) in SP2 and SP4, respectively. SO_2 and NO_x are in the range of 20 to 50 mg/Nm^3 and sometimes shoot up to 200 to 450 mg/Nm^3.
4. Due to the limited capability of the stack monitoring instrument, the content of SO_3 and its effect could not be ascertained separately.
5. Data analysis of SEM results indicated the presence of sinter components as the trapped particles. Chlorides remained in the matrix.
6. The particulates entrapped in the thimbles in the cases of MEROS and HTBF contained KCl, NaCl in the matrix, SO_2, NO_x in minor quantities, and sinter components. In the case of ESP, the SO_2 particles are in minor quantities; the chlorides and sinter components are dominated. The presence of a high amount of NO_x in the case of ESP is confirmed by SEM results.
7. $PM_{2.5}$ escaped the MEROS, HTBF, and the thimbles too.
8. In all the cases, the size of the particulates determined whether they are appearing in the stack or not. The VOCs, PCDD/Fs might have escaped into the atmosphere as they are too tiny particles. After the annual maintenance is carried out on the ESPs and bag filters, their performance will improve. A state-of-the-art fabric filter that can trap $PM_{2.5}$ is suggested as a one-time solution in the sinter plant without a bag filter.

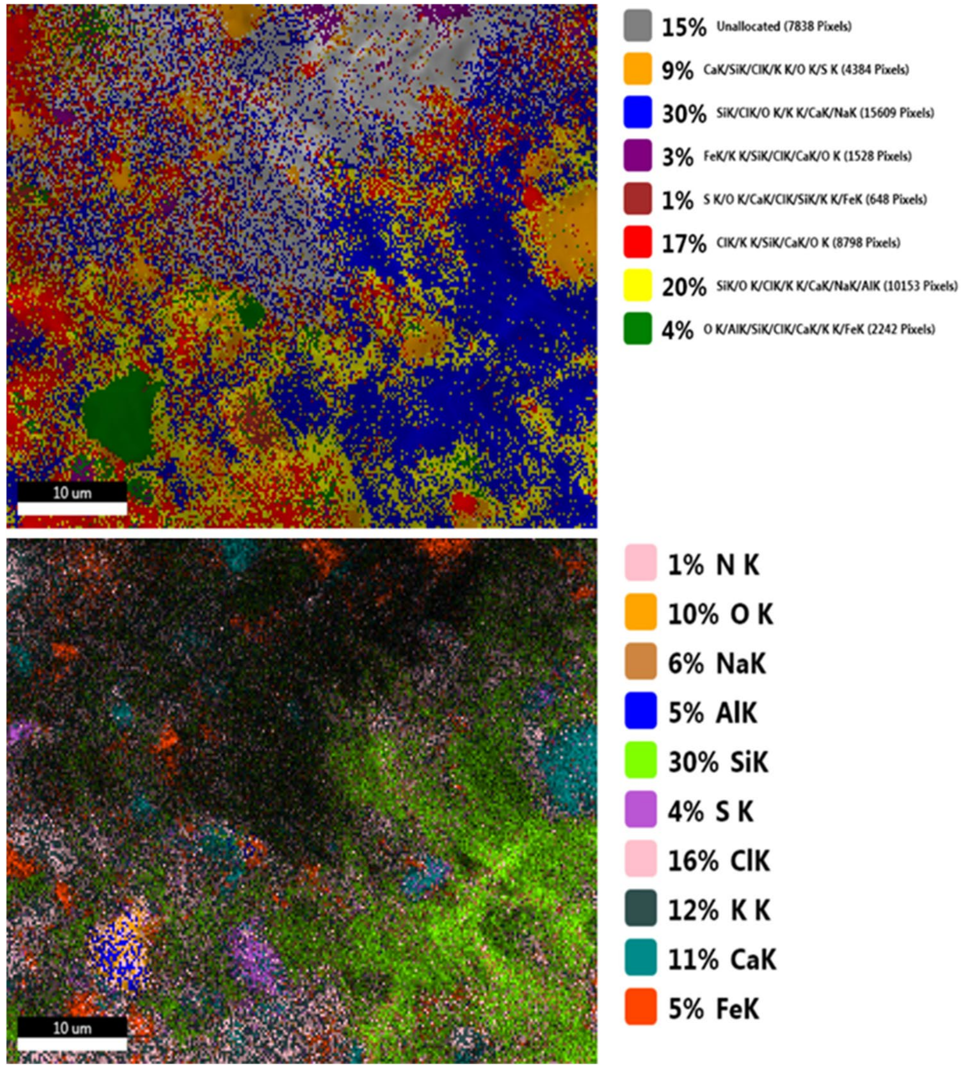

Fig. 18 Mapping of the ESP thimble

Table 5 Elemental analysis (at%) of the MEROS thimble

Element	N K	O K	NaK	AlK	SiK	S K	ClK	K K	CaK
1	7.13	67.63	6.95	1.07	9.75	0.67	0.48	0.70	5.61
2	5.37	67.38	4.46	0.50	9.33	0.70	0.50	1.16	10.59
3	10.27	63.34	4.21	0.82	2.75	1.08	0.95	0.71	15.88
4	10.16	48.25	26.92	0.18	5.02	1.43	4.21	1.13	2.71
5	7.48	56.87	7.62	1.08	21.8	0.37	0.28	0.68	3.83
6	8.67	72.33	7.24	1.35	4.54	0.83	0.54	0.75	3.75

Table 6 Elemental analysis (at%) of the HTBF thimble

Element	N K	O K	NaK	AlK	SiK	S K	ClK	K K	CaK	FeK
1	3.68	26.04	3.52	1.45	9.21	3.46	20.48	20.88	5.12	6.16
2	12.26	53.82	3.30	7.41	6.26	1.32	4.67	7.84	0.83	2.30
3	2.75	21.33	3.20	1.22	7.96	3.47	31.54	20.23	3.89	4.40
4	4.26	22.68	3.20	1.15	7.63	3.47	17.47	32.63	3.41	4.11
5	6.78	40.81	1.51	1.79	2.33	1.23	4.33	4.15	4.37	32.68
6	0.45	24.94	4.45	1.65	25.46	3.05	16.71	15.78	4.04	3.47
7	1.51	23.60	4.28	1.83	12.63	4.25	15.95	18.35	7.83	9.78
8	5.27	32.74	3.77	1.81	5.95	4.54	14.40	13.33	13.15	5.04

Table 7 Elemental analysis of ESP thimble

Element	N K	O K	NaK	AlK	SiK	S K	ClK	K K	CaK	FeK
1	4.98	46.41	5.32	1.94	13.33	1.39	7.94	6.25	6.83	5.61
2	0.03	36.48	1.91	0.08	14.54	0.57	10.73	10.09	12.06	13.51
3	6.70	47.18	2.03	1.52	5.24	2.00	5.94	4.71	20.04	4.65
4	2.58	41.37	7.76	0.99	27.4	0.68	7.18	4.53	5.10	2.39
5	1.36	25.62	2.63	0.99	6.35	0.97	6.62	7.17	5.38	42.89
6	6.74	55.89	2.60	1.35	3.60	7.42	4.33	3.23	9.34	5.50
7	5.76	41.51	3.61	1.01	7.67	1.64	15.67	11.43	5.60	6.11
8	5.72	48.35	6.83	1.70	11.78	1.53	6.84	6.85	5.24	5.16
8	9.72	61.42	1.98	9.19	2.73	1.22	3.05	2.69	2.86	5.14

Acknowledgments The authors express their gratitude to the teams of Environmental Laboratory and R&D departments for their support in conducting the investigation and characterization of the particulates.

Declarations

Conflict of interest The authors declare that they have no conflict of interest.

References

1. Craig F, Bohren DRH (1983) Absorption and scattering of light by small particles. Wiley, New York
2. Abreu GC, Ferreira A-M-M, Oliveira H-L-M et al (2007) Visibility control of main stack plume at CST sinter plant: a scientific approach. Rev Métall 104:380–383. https://doi.org/10.1051/metal:2007202
3. Kasama S, Kitaguchi H, Yamamura Y et al (2006) Analysis of exhaust gas visibility in iron ore sintering plant. ISIJ Int 46:1027–1032. https://doi.org/10.2355/isijinternational.46.1027
4. Poole D, Aries E, Ciaparra D et al (2011) Investigations into the parameters influencing plume visibility at UK sinter plants. In: 2nd International conference and exhibition clean technologies in the steel industry, 26–28 September 2011, Budapest, pp 279–290
5. Ji Z, Fan X, Gan M et al (2017) Influence of sulfur dioxide-related interactions on PM 2.5 formation in iron ore sintering. J Air Waste Manage Assoc 67:488–497. https://doi.org/10.1080/10962247.2016.1259692
6. U.S. Environmental Protection Agency (1996) Addendum to the user's manual for the plume visibility model, PLUVUE-2 (Revised)
7. Angalakuditi VB, Gujare R, Anbarasu R et al (2022) Characterization and in situ abatement of SOx, NOx, and PCDD/Fs in iron ore sinter machine wind legs. J Sustain Metall. https://doi.org/10.1007/s40831-022-00524-w
8. Tyndall J (2022) Tyndall effect. Wikipedia. https://en.wikipedia.org/wiki/Tyndall_effect
9. Sidebottom HW, Badcock CC, Jackson GE et al (1972) Photooxidation of sulfur dioxide. Environ Sci Technol 6:72–79. https://doi.org/10.1021/es60060a001
10. Li J, Li K, Zhang H et al (2022) Effects of OH radical and SO_2 concentrations on photochemical reactions of mixed anthropogenic organic gases. Atmos Chem Phys 22:10489–10504. https://doi.org/10.5194/acp-22-10489-2022
11. U.S. Environmental Protection Agency (1978) Pollution effects of abnormal operations in iron and steel making—vol II. Sintering, Manual of Practice. Washington DC
12. ThyssenKrupp Steel (2020) Thyssenkrupp starts operation of the world's biggest fabric filter for the sintering process. ThyssenKrupp's Newsroom. https://www.thyssenkrupp-steel.com/en/newsroom/highlights/fabric-filter.html

Publisher's Note Springer Nature remains neutral with regard to jurisdictional claims in published maps and institutional affiliations.